Int. J. Electrochem. Sci., 14 **(2019)** 8216 – 8227, doi: 10.20964/2019.08.95

International Journal of
ELECTROCHEMICAL
SCIENCE
www.electrochemsci.org

Preparation of High Specific Surface Area Activated Carbon from Black Wolfberry Branches as an Efficient Electrode Material for Supercapacitors

Gaofeng Shi[*], *Qi Zhang, Chao Liu, Guoying Wang, YucanDong, Zhao Wang, Hongquan Zhang, PengZhang, Fenfang Luo，Xin Li*

School of Petrochemical Engineering, Lanzhou University of Technology,
NO.287, Lan gong ping Road, Lanzhou, Gansu, China
[*]E-mail: gaofengshi_lzh@163.com

Received: 7 April 2019 / *Accepted:* 11 June 2019 / *Published:* 30 June 2019

Black wolfberry branches are used as raw materials, and the KOH activation method is adopted for producing activated carbons with a high specific surface area. The characterization of the material reveals that with increasing activation temperatures, the specific surface area (SSA) and interconnected microporous/mesoporous structure are augmented. The SSA of the prepared material reaches 2046.07m^2 g^{-1} and a high pore volume of 0.7cm^3 g^{-1} is obtained. Furthermore, the prepared material exhibits excellent electrical performance. As an electrode material, the specific capacitance is as high as 355.7F g^{-1}. at a current density of 1 A g^{-1}, and the capacitance loss rate is 6.4% after 5000 cycles of charging and discharging at a current density of 2 A g^{-1}. These findings indicate that the wolfberry branch is a kind of biomass material, especially suitable for the preparation of super-activated carbon.

Keywords: Black wolfberry branches; supercapacitors; electrode materials; electrochemical performance

1. INTRODUCTION

With rapidly decreasing fossil fuels and the increasing demand for energy, it is extremely urgent to develop and utilize renewable energy sources and study new energy storage devices. Supercapacitors are a new type of energy storage device that have attracted extensive attention because of their short charging time, reliable cycle stability, good temperature characteristics, energy savings and environmental friendliness [1, 2]. The core of the supercapacitor design is to find suitable electrode materials. Carbon materials, metal oxides, conductive polymers, etc. are often used as

electrode materials for supercapacitors. Carbon materials are favoured by researchers because of their simple preparation process, low cost, and wide source of raw materials.

As a member of the carbon material family, activated carbon is the earliest electrode for the assembly of supercapacitors. The preparation process of activated carbon is relatively mature. Therefore, many fields have higher requirements for the specific surface area of activated carbon, and researchers have paid more attention to the preparation and application of super-activated carbon with a specific surface area over 2000 m^2 g^{-1}. Traditionally, activated carbon (AC) has been prepared mainly from coal, petroleum and their derived products [3, 4]. However, these resources are non-renewable and exist in a finite amount. Additionally, using these resources facilitates environmental problems. Thus, researchers have been investigating new carbon sources. Due to its low cost, renewable nature, ease of availability and environmental friendliness, agricultural residuals have always been the focus of researchers working in the carbon field. AC has been previously synthesized from various agricultural residues such as: walnut shells [5], bamboo [6], orange peel [7], rotten carrot [8], sugar cane bagasse [9], tea leaves [10], nut shells [11], cotton stalk [12] and coconut shells [13]. Many biomass sources, such as wood chips and nut shells, have also been used in the production of activated carbon. Huang et al. [14] prepared super-activated carbon with a specific surface area of up to 3400m^2 g^{-1} by a chemical activation method using a litchi trunk as the raw material and KOH as the activator. Jin et al. [15] obtained activated carbon from corn stover by microwave radiation and slow pyrolysis, and the specific capacitance reached 245.9 F g^{-1} at 0.1 A g^{-1}.

Wolfberry is a Solanaceae plant mainly distributed in Ningxia, Gansu, Qinghai and other western regions of China. The fruit has high medicinal value, but the pruned branches are often burned or discarded. This kind of waste not only reduced the utilization rate of wolfberry, but also increased environmental pollution. The use of discarded wolfberry branches as a carbon source for AC synthesis increases the added value of biomass energy, which has far-reaching significance for rural development in western China. In this paper, super-activated carbon material is prepared through carbonization and KOH activation of the wolfberry branches. By materials characterization, the maximum specific surface area of the activated carbon can reach 2046.07 m^2 g^{-1}, and when the mass ratio of KOH to raw material is 3:1, the activation time for 120 min and the activation temperature at 900 ℃, the activated carbon material WB-900 exhibits a high specific capacitance of 355.7 F g^{-1} at 1A g^{-1}. This results indicates that the wolfberry branch is a kind of biomass material especially suitable for the preparation of super-activated carbon.

2. EXPERIMENTAL

2.1. Materials

The raw material (black wolfberry branches) used in the present study was collected from Xi-ning, Qinghai Province, China. KOH and HCI were purchased and used without further purification.

2.2. Preparation of activated carbon

The raw material was repeatedly washed with deionized water to remove impurities and then was dried in an oven at 100 °C overnight. The next morning, the dried wolfberry branches (WBs) were pulverized and sieved with a 100-mesh standard sieve. WB-based activated carbon (AC) was synthesized by employing a standard chemical activation method. The process can be described as follows: carbonization, activation, and water washing (the washing process was mainly to wash away part of the alkali in the activated carbon, to reduce the amount of hydrochloric acid in the pickling process), pickling and washing. Fig. 1 shows the flow chart of the preparation of wolfberry branch-based super-activated carbon by the KOH activation method. First, wolfberry branch powder was carbonized in a tube furnace. Carbonization occurred, at 600 °C, for 2 h while, heating at 5 °C•min^{-1}, with a nitrogen flow of 1.5 NL•min^{-1}, and the initial carbon product was obtained. The carbon products and KOH were prepared into a mixture of KOH/carbon products according to a mass ratio of 1:4. The mixture was then successively placed in a porcelain boat, loaded in a tubular furnace and heated at 700 ～1000 °C for 2 h under N_2 atmosphere. After activation, the porcelain boat was removed and cooled to room temperature. After initial washing with deionized water, the samples were washed with 0.1 mol·L^{-1} hydrochloric acid to neutral, and then fully washed with deionized water. Finally, the activated carbon obtained by washing was dried for 12 h at 95 °C in a vacuum oven, and marked as WB-x (x represents the carbonization temperature). Additionally, to demonstrate the excellent capacity performance of the activated microporous carbons, we used unactivated biomass carbon as a control sample (referred to as WB).

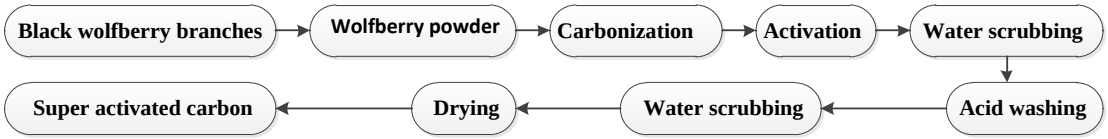

Figure 1. Flow diagram of preparation of wolfberry branches-based activated carbon

2.3 Activated carbon Structure characterization

The morphology and microstructure of the activated carbon was observed by cold field emission scanning electron microscopy (SEM, JSM-6701FJapan Electron Optics Co., Ltd.) and transmission electron microscopy (TEM, JEOL JEM-2010, Japan). The surface areas and pore size distributions of all samples were measured by N_2 adsorption and desorption at 77 K using a Micromeritics ASAP 2020 automatic analyser (USA). X-ray diffraction patterns (XRD) were obtained using an MSAL-XD2 diffractometer in the diffraction angle scanning range of 5° to 80°. The crystallographic structures of activated carbons were characterized by Raman spectroscopy (JYHR800, Micro-Raman). The surface elemental composition was tested with X-ray photoelectron spectroscopy (XPS, PHI5702, USA).

2.4 Electrochemical measurements

The electrochemical capacitive performance of WB-x was evaluated and compared on a CHI660E electrochemical workstation (CHI660E, Shanghai Chenhua Instrument Co., Ltd.) in a 6 M KOH electrolyte solution with a three-electrode configuration. For preparing the working electrodes, a slurry was obtained by mixing acetylene black (15 wt.%), prepared material (80 wt.%) and polytetrafluoroethylene (5 wt.%). The slurry was then covered onto a 2.0 cm×1.0 cm of foamed nickel to prepare electrodes. Prior to use, the prepared electrode was dried for 12 h at 80°C in a vacuum and then pressed at 5 MPa for 2 min. In the three-electrode test system, cyclic voltammetry (CV), galvanostatic charge–discharge (GCD), and impedance (EIS) were performed on an electrochemical workstation using a saturated calomel electrode (SCE) and a platinum foil as a reference electrode and a counter electrode, respectively. When a 6 M KOH solution was used as an electrolyte, the cyclic voltammetry (CV) curve test was performed by changing the scanning rate from 5 $m \cdot Vs^{-1}$ to 100 $m \cdot Vs^{-1}$. Electrochemical impedance spectroscopy (EIS) and galvanostatic charge–discharge (GCD) tests were performed using a computer-controlled CHI660E electrochemical workstation in the frequency range of 0.1 Hz to 100 kHz. The specific capacitance, energy density and power density of the fabricated samples were calculated as follows:

$$\mathrm{C} = \frac{I\Delta t}{m\Delta V} \quad (1)$$

$$\mathrm{E} = \frac{1}{2} C \Delta V^2 \quad (2)$$

$$\mathrm{P} = \frac{E}{t} \quad (3)$$

where I denotes the discharge current (A), m (g) is the mass load, Δt(t) is the discharge time, ΔV(V) is the potential window of the discharge, E is the energy density and P is the power density [16, 17].

3. RESULT AND DISCUSSION

Wolfberry branches have a higher cellulose content and cellulose in plant tissue can be easily converted to carbon at a high temperature. The SEM images of the wolfberry branches activated by KOH at 900 ℃ are shown in Fig. 2 (a). As shown in the figure, after high temperature activation by KOH, the material exhibits an irregular block structure, and the outer surface is rough, but there are no obvious pore structures. The mesoporous structure is gradually consolidated because of the increase in the activation temperature. As shown in Fig. 2b, a large number of micropores were observed in the activated carbon material, and the presence of these micropores promoted electrolyte penetration and provided more electrochemical sites, which can improve the transport of ions and electrochemical properties [18, 19]. At the same time, these micropores provide a large specific surface area for the prepared carbon material. The N_2 adsorption/desorption isotherms (Fig. 2c) and pore size distribution

(Fig. 2d) were further investigated to determine the specific surface area and porosity characteristics of biomass carbon activated by KOH. As shown in Fig.2(c), all the WB-x materials possess a high N_2 sorption capacity and display a type-I sorption isotherm characteristic. The steep increase in volume adsorption occurs at a low relative pressure (P/P 0 < 0.05), indicating the presence of abundant micropores (pore width <2 nm) [18]. As the activation temperature increased from 700 ° C to 900 ° C, the specific surface area and total pore volume of the carbon material gradually increased, indicating that the temperature had a large influence on the specific surface area of the prepared sample. When the temperature reaches 1000 °C, because the temperature is too high to cause excessive activation of raw materials, the tunnel collapses, leading to a decrease in the specific surface area. Furthermore, the pore size distribution reveals that the micro-mesopores of WB-800 and WB-900 have a broader size distribution than those of WB-700 and WB-1000 (Fig.2d). Table 1 reveals that the specific surface areas of WB-x are much higher than those of WB. For WB-x, the volume and specific surface area increase with increasing x to some extent due to the formation of pores by KOH etching, while WB-1000 was different from the other samples. This feature of WB-1000 could be related to the excessive activation of black wolfberry branch-derived carbon by high temperature causing the collapse of the etching pores and leading to a decrease in the volume and specific surface area. As listed in Table 1, the specific surface area of WB-900 (2046.07 m^2 g^{-1}) was the highest among the four samples (WB-700, WB-800, WB-1000). Meanwhile, the total pore volume of WB-900 (0.99 cm^3g^{-1}) is also higher than those of others. The above results showed that the WB-900 is a good electrode material.

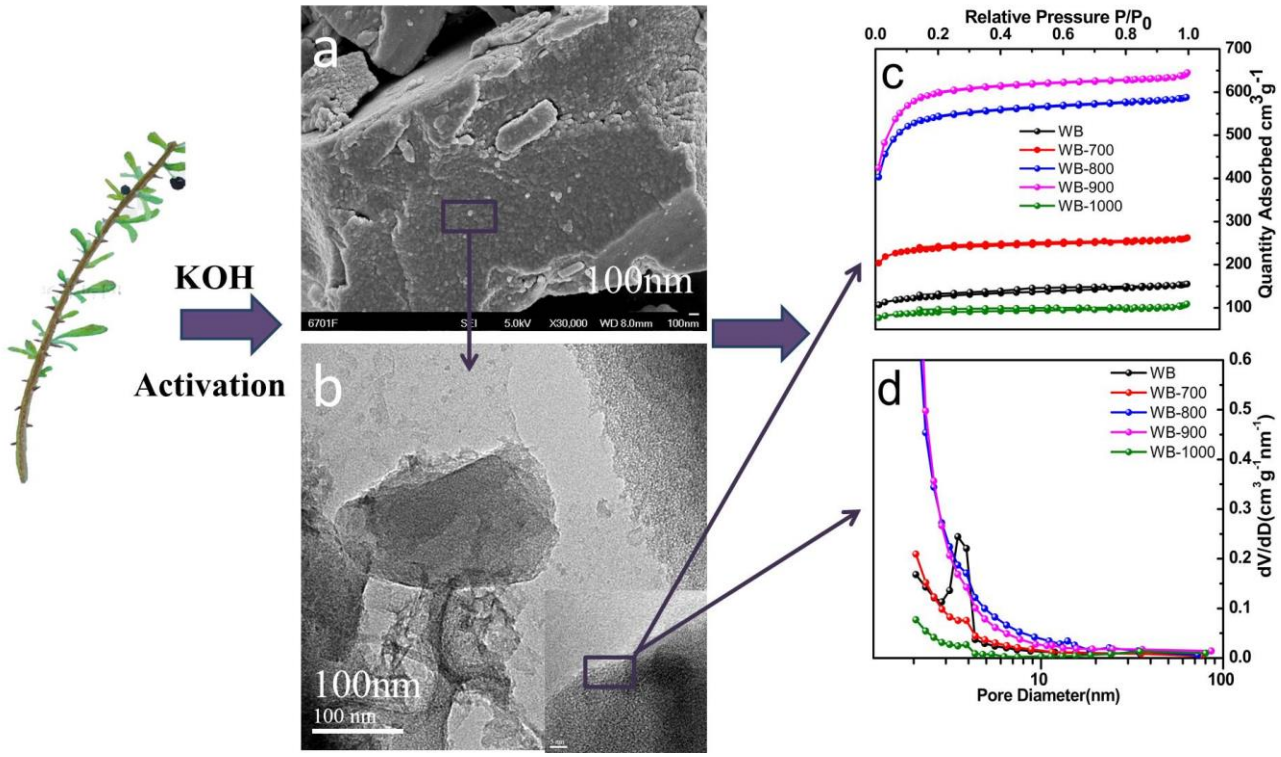

Figure 2. SEM(a) and TEM(b) micrographs of sample WB-900; nitrogen adsorption/desorption isotherms (c) and pore size distributions curves(d) of the WB samples.

Table 1. Pore size distribution of porous carbon

Sample	S_{BET} $cm^2 \cdot g^{-1}$	V_t $cm^3 \cdot g^{-1}$	D_{av} nm	V_{mi} $cm^3 \cdot g^{-1}$	V_{me} $cm^3 \cdot g^{-1}$	S_{mi} $cm^2 \cdot g^{-1}$	S_{me} $cm^2 \cdot g^{-1}$
WB	430.01	0.24	2.20	0.14	0.10	304.43	125.58
WB-700	799.84	0.40	2.00	0.31	0.09	663.60	136.24
WB-800	1855.55	0.90	1.95	0.66	0.24	1442.53	413.02
WB-900	2046.07	0.99	1.93	0.70	0.29	1529.12	516.95
WB-1000	301.88	0.16	2.12	0.11	0.05	240.39	61.49

S_{BET}: total BET specific surface area, S_{me}: mesopore specific surface area, S_{mi} : micropore specific surface area, D_{av}: average pore diameter, V_t: total pore volume, V_{me}: mesoporous volume, V_{mi}: microporous volume.

The XRD patterns of the prepared materials and their pre-cursors are shown in Fig. 3(a). All the materials exhibit two broad peaks at approximately 22° and 43.9° corresponding to the diffraction of the (002) and (100) planes of the graphitic frameworks [20]. Broad characteristic peaks appeared at 22° for the five samples, corresponding to the (002) crystal plane. These peaks indicate a disturbed structure due to the randomly oriented aromatic carbon sheets in the obtained carbons, which is a major factor for the high specific surface area [21]. The other broad peak, located at approximately 43.9°, may be attributed to the amorphous carbon (100) crystal plane of the graphite layer, which is suggested for improving the electrical conductivity of carbon [22].

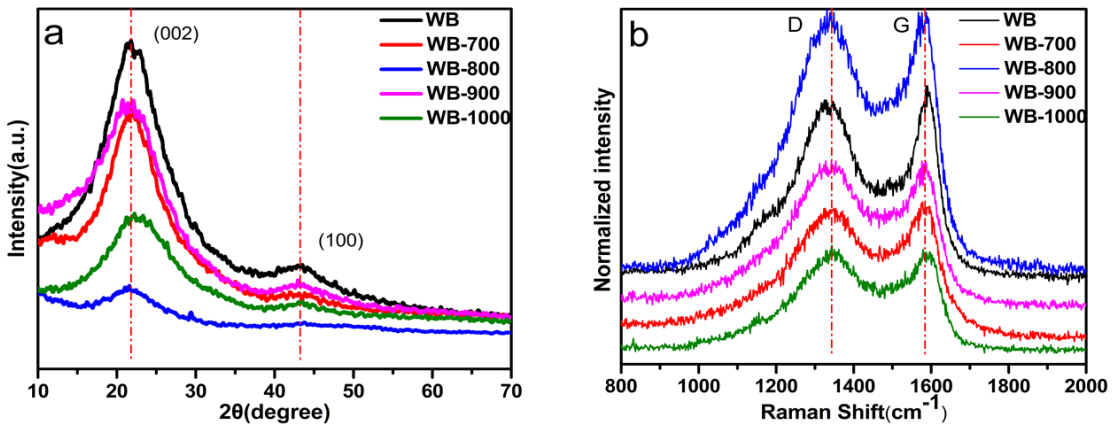

Figure 3. (a) XRD patterns of WB-x samples, (b) Raman spectrum of WB-x samples.

In addition, no diffraction peaks of other elements were found except for the diffraction peak of carbon, which shows that the activated carbon prepared by the method has less impurities and high purity. Raman spectroscopy was further employed to analyse the microstructure of the activated biomass carbons and their precursors. Two characteristic peaks are clearly observed in Fig. 3(b). The two characteristic diffraction peaks are located at 1340 cm^{-1} (D band) and 1590 cm^{-1} (G band). The D

band represents the defect of the C atomic lattice, which is related to the existence of the disordered carbon structure, while the G band represents the in-plane stretching vibration of the sp^2 hybrid carbon atoms [23]. In general, the intensity ratio of D and G bands (I_D/I_G) can be used to reflect the degree of structural disorder and graphitization in carbon materials [24]. The I_D/I_G of the WB, WB-700, WB-800, WB-900, and WB-1000 samples are 0.93, 0.96, 1.02, 1.00, and 1.03, respectively. The above data show that as the activation temperature increases, the disorder of the atomic arrangement increases and the degree of graphitization decreases.

The composition of the organic elements and their bond configuration of WB-900 was further analysed by XPS. As shown in Fig. 4a, the XPS spectrum showed that the as-prepared activated carbon was predominantly composed of carbon and oxygen. Among them, the C content was 90.32 wt%, the O content was 8.99 wt%, the N content was 0.68 wt%, and the P content was 0.01 wt%. This finding indicates that the content of elemental N and P of the porous carbon is small. The peaks at 285 and 520 eV in full spectra correspond to the C1s and O1s, respectively. The curve of the C1s level peak of the XPS spectrum can be fitted into four parts, including the C=C (284.5 eV), C-O-C (286 eV), C-O (286.7 eV) and C=O (289 eV) bonds [25, 26], respectively (Fig. 4b). As shown in Fig. 4c, the curve fitting of the O1s spectrum was divided into three peaks: C=O(531.6 eV), C-O(532.7 eV) and O=C-O(533.7 eV) bonds [27]. The presence of these oxygen-containing functional groups indicates that the prepared electrode material contains functional carbon [27, 28].

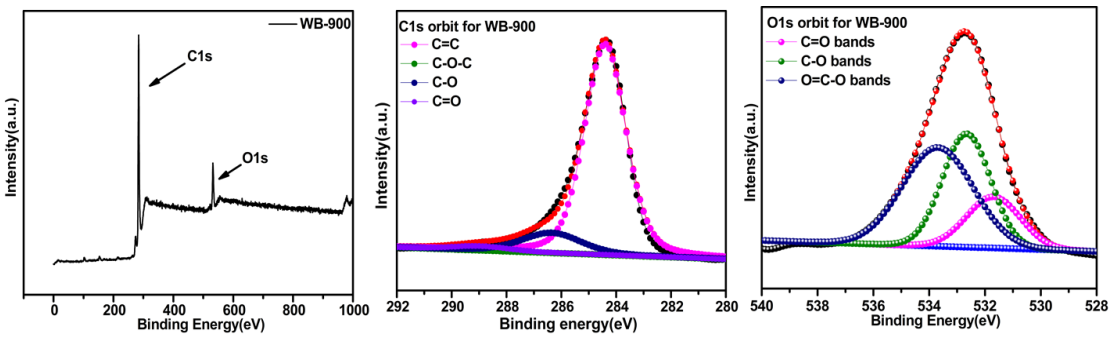

Figure 4. High-resolution XPS spectra of full peak, C1s and O1s orbits for the fabricated WB-900 sample

The electrochemical performances of the WB-x series samples were evaluated in a three-electrode system. As shown in Fig. 5(a), the CV curves of the WB-x series samples exhibit a quasi-rectangular shape at a scan rate of 20 $mV \cdot s^{-1}$, typical of electrical double-layer capacitors. It can be seen from the figure that the CV curve area of biomass carbon after KOH activation is much higher than that of unactivated biomass carbon. This may be because the activation increases the BET specific surface area, while the high specific surface area and pore size structure can influence the specific capacitance and rate performance of the sample. The WB-900 electrode has the highest surrounding area in the CV curve compared to the other samples, indicating that WB-900 has the highest specific capacitance. This result indicates that 900 ℃ is the best activation temperature. The discharge curves of the prepared sample at 1 $A \cdot g^{-1}$ are shown in Fig. 5(b). As shown in the figure, all GCD patterns

exhibited symmetrical triangles and were closely linear, in accordance with the characteristics of the ideal electric double layer capacitor constant current curve. At a current density of 1 A•g^{-1}, the specific capacitances tested for WB, WB-700, WB-800, WB-900, and WB-1000 were 98.6 F•g^{-1}, 170.4 F•g^{-1}, 297.6F•g^{-1}, 355.7F•g^{-1} and 197.7 F•g^{-1}, respectively. The results showed that the discharge time of the CP curve increases with increasing temperature, and the specific capacitance decreases after 900 °C. This finding is consistent with the results of the specific surface area tests, indicating that the specific surface area is an important parameter for the performance of the electrochemical capacitor. Fig. 5(c) shows the cyclic voltammogram of the WB-900 sample at different sweep speeds. It can be seen from the figure that the shape of the curve shows no significant change when the scanning rate is increased from 5 mV•s^{-1} to 100 mV•s^{-1}, indicating that the sample material exhibits good capacitive behaviour. At the same time, there is no redox peak in the volt-ampere cycle curve. This curve showed that there was almost no pseudo-capacitance in the sample material, and the electrode reaction was mainly a double layer charge transfer reaction, which was also a characteristic of the typical double-layer capacitor. Fig. 5(d) shows the galvanostatic charge-discharge curves of the WB-900 samples at different current densities. When the current density increased from 1 A•g^{-1} to 10 A•g^{-1}, the specific capacitance could still be maintained at 281 F•g^{-1}. These results indicate that the sample has excellent columbic efficiency and good electrochemical reversibility during the process of charging/discharging storage. The specific capacitance of the samples at different current densities are presented in Fig. 5(e) and Table 2. When the current density increases from 1 A·g^{-1} to 10 A·g^{-1}, the specific capacitance retention rate is 81.1% for WB, 75.1% for WB-700, 82% for WB-800, 79% for WB-900, and 79.1% for WB-1000. Although WB-900 has a high specific capacitance, its capacitance retention rate is not the highest. This result may be due to the good rate performance determined by the combination of the appropriate specific surface area and the stability of the material structure. Compared with WB-900, the capacitance of WB-800 and WB-1000 decreased, corroborating that only appropriate specific surface area and pore sizes can improve the electrochemical properties [29]. Electrochemical impedance spectroscopy can evaluate the conductivity, charge transfer and other properties of the electrode [30]. Fig. 5(f) shows an EIS spectrum of the five samples in a three-electrode system. It can be seen from the figure that the Nyquist plot of all sample electrodes is almost vertical in the low frequency region. At the same time, the slope of the curve of the WB-900 sample electrode is significantly larger than that of the other sample electrode, indicating that the electrolyte solution has better diffusion performance in the WB-900 sample. All samples produced a small semi-circular Faraday impedance arc in the high frequency region, and the measured equivalent resistances are 0.5716 Ω for WB, 1.834 Ω for WB-700, 0.918 Ω for WB-800, 0.718 Ω for WB-900, and 1.5 Ω for WB-1000, which are generally low and indicate that the carbon materials demonstrate the desired capacitive behavior. The energy and power densities for the different samples under different current densities are presented in Fig. 5 (g). The electrode material WB-900 delivers a high energy density of 49.4 W.h kg^{-1} at a power density of 500 W kg^{-1}, which is larger than other electrode materials in the present study.

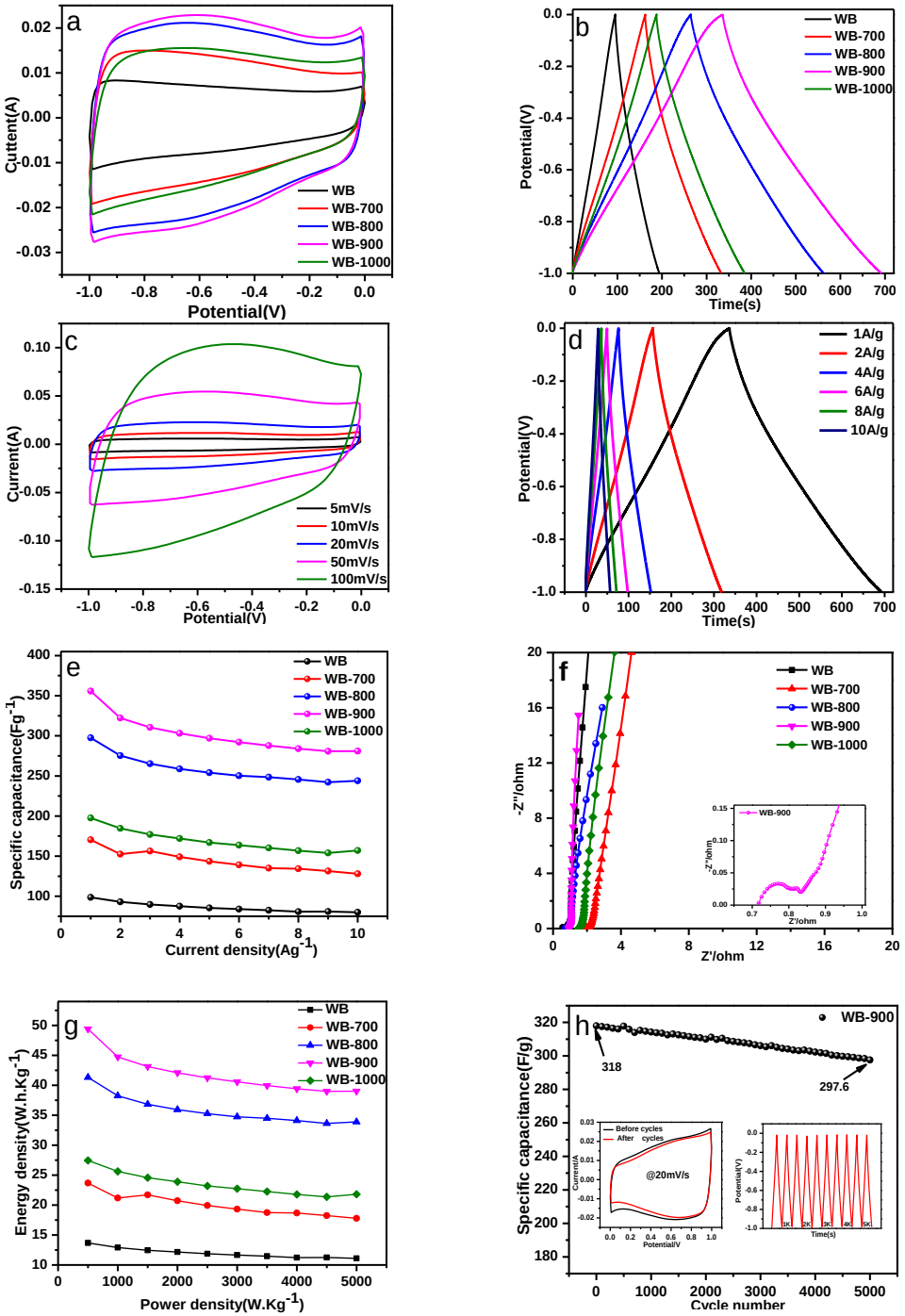

Figure 5. Electrochemical performance of the samples measured in a three-electrode system. (a) CV curves for all the samples at a scan rate of 20 mV•s^{-1}; (b) galvanostatic charge-discharge curves of all the samples at a current density of 1 A•g^{-1}; (c) CV curves for WB-900 at scan rates ranging from 5 mV•s^{-1} to 100 mV•s^{-1}; (d) galvanostatic charge-discharge curves of WB-900 at different current densities; (e) specific capacitance of the samples versus various current densities from 1 A•g^{-1} to 10 A•g^{-1}; (f) Electrochemical impedance spectra(EIS) of the WB-900; (g) Energy and power density of five samples, (h) WB-900 in specific capacitance retention rates at the current density of 2 A•g^{-1} after 5000 cycle.

The prepared electrode material emits the strongest electric energy through the electrolyte reaction at 900 °C. Fig. 5 (h) shows that WB-900 has excellent cycle stability at a current density of 2 $A•g^{-1}$ in a 6 M KOH electrolyte. It can be seen from the figure that after 5,000 cycles of charge and discharge, the specific capacitance of WB-900 is 297.6 $F•g^{-1}$ and the retention rate is 93.6%.

The CV curves showed almost no significant change before and after 5000 cycles at 20 $mV•s^{-1}$ (inset in Fig. 5 (h) left), and the GCD curves still showed symmetric triangular shapes in the cycling test process (inset in Fig. 5(h) right), demonstrating that the sample of WB-900 is a good supercapacitor electrode material.

Table 2. Specific capacitance of porous carbon ($F•g^{-1}$)

Current density ($A·g^{-1}$)	1	2	4	6	8	10
WB	98.6	93	87.6	84	80.8	80
WB-700	170.4	152.6	149.2	135	134.4	128
WB-800	297.6	275.4	258.8	250.2	245.6	244
WB-900	355.7	322.2	303.2	292.2	284	281
WB-1000	197.7	184.6	172	163.8	156.8	157

Table 3. Comparison of electrochemical performance of porous carbon with other different materials

Electrode materials	Specific capacitance(current density	S_{BET} ($m^2\ g^{-1}$)	Electrolyte	Referencces
Hierarchically porous carbon derived from waste tea-leaves	330 F g^{-1} (1A g^{-1})	2245 $m^2\ g^{-1}$	2 Mol L^{-1} KOH	［10］
Hierarchically porous carbon derived from corn stover	211 F g^{-1} (0.1A g^{-1})	1432 $m^2\ g^{-1}$	6 Mol L^{-1} KOH	［15］
Hierarchically porous carbon derived from rice husk ash	260 F g^{-1} (1A g^{-1})	786 $m^2\ g^{-1}$	6 Mol L^{-1} KOH	［18］
Hierarchically porous carbon derived from black wolfberry branches	355 F g^{-1} (1A g^{-1})	2046 $m^2\ g^{-1}$	6 Mol L^{-1} KOH	This work

4. CONCLUSIONS

Activated carbon was prepared by the KOH chemical activation method with wolfberry branches as the raw material. This carbon material exhibited a well-developed void structure, a large

specific surface area and a larger pore volume. Meanwhile, the morphology, microstructure and electrochemical properties of porous carbon under different activation temperatures were investigated. By controlling the temperature, sample WB-900 demonstrated the best electrochemical performance. The activated carbon material WB-900 exhibits a high specific capacitance of 355.7 F g^{-1} at 1A g^{-1} in a three-electrode system with a 6 M KOH electrolyte. When the current density was 1 A•g^{-1}, the energy density was 49.4 Wh•kg^{-1}, the power density was 500 W•kg^{-1}, and the capacitance retention rate was 79%, which demonstrates good rate performance. It has been shown that wolfberry branch-derived porous carbon materials have exciting commercial potential as electrodes for supercapacitors.

ACKNOWLEDGEMENTS
This work was supported by the National Natural Science Foundation of China (21567015), the National Key Research and Development Program of China (2016YFC0202900), Lanzhou university of technology hongliu first-class discipline construction program and Lanzhou university of technology Hongliu Science Fund for Young Scholars (2018).

References

1. X. Zhao, P. Li, S. W Yang, Q. Z. Zhang and H.M. Luo, *Ionics*, 23(2017)1239.
2. C. Lu, Y.H. Huang, Y.J. Wu, J. Li and J.P. Cheng, *J. Power Sources,* 394(2018)9.
3. M.X. Wang, Q. Liu, H.F Sun, E.A. Stach, H.Y. Zhang, L. Stanciu and J.Xie, *Carbon,* 50(2012) 3845.
4. K. Jost, D. Stenger, C.R. Perez, J. Mcdonough, K. Lian, Y. Gogotsi and G. Dion, *Energy Environ. Sci.*, 6(2013)2698.
5. S. Cheng, L.B. Zhang, H.Y. Xia, J.H. Peng, S.Z. Zhang and S.X. Wang, *J. Porous Mater*., 22(2015) 1527.
6. Q.S. Liu, T. Zhen, P. Wang and L Guo, *Ind. Crop Prod.*, 31(2010) 233.
7. A.E. Nemr, O. Abdelwahab, A. EI-Sikaily and A. Khaled, *J. Hazard Mater.*, 161(2009) 102.
8. S. Ahmed, A. Ahmed and M. Rafat, *J. Saudi Chem. Soc.*, 22(2018) 993.
9. N.K. Amin, *Desalination*, 223(2008)152.
10. C. Peng, X.B. Yan, R.T. Wang, J.W. Lang, Y.J. Ou and Q.J. Xue, *Electrochim. Acta*, 87(2013)401.
11. A.C. Lua and T. Yang, *J. Colloid Interface Sci.*, 290(2005)505.
12. B.S. Girgis, and M.F. Ishak, *Mater. Lett,*. 39(1999)107.
13. Z.H. Hu and M.P. Srinivasan., *Micropor Mesopor Mat.*, 27(1999)11.
14. C.C. Huang, H.M. Chen and C.H. Chen, *Int. J. Hydrogen Energy,* 35(2010) 2777.
15. H. Jin, X.M. Wang, Y.B. Shen and Z.R. Gu, *J. Anal & Appl Pyrol*, 110(2014)18.
16. H. Chen, Y.C. Guo, F. Wang, G. Wang, P.R. Qi, X.H. Guo, B. Dai and F. Yu, *New Carbon Mater.*, 32(2017)592.
17. R.B. Qiang, Z.G. Hu, Y.Y. Yang, Z.M. Li, N. An, X.Y. Ren, H.X. Hu and H.Y. Wu, *Electrochim Acta*, 167(2015) 303.
18. Y.Q. Huang, J. He, Y.T. Luan, Y. Jiang, S.E. Guo, X.G.Zhang, C.G. Tian and B.J. Jiang, *Rsc. Adv.*, 7(2017) 10385.
19. L. Peng, Y.R. Liang, H.W. Dong, H. Hu, X. Zhao, Y.J.Cai, Y. Xiao, Y.L. Liu and M.T. Zheng, *J. Power Sources,* 377(2018)151..
20. T. Yuan, E.H. Liu, R. Ding, K. Liu, R.H. Liu, L. Wang, Z. Yang and H.X. Jiang, *Electrochim Acta*, 194(2016)394.
21. L. Zhang, F. Zhang, X. Yang, K. Leng, Y. Huang and Y.S. Chen, *Small*, 9(2013)1342.
22. J.P. Paraknowitsch, Y.J. Zhang, B. Wienert and A. Thomas, *Chem. Commun.*, 49(2013)1208.
23. D.Y. Zhang, M. Han, Y.B. Li, J.J. He, B. Wang, K.J. Wang, H.X. Heng, *J. Power Sources,*

372(2017)260.
24. C. Ma , J.L. Shi , Y.J. Li , Y. Song and L.Liu, *Carbon*, 95(2015)1082.
25. Z.Y. Lin, G. Waller, Y. Liu, M.L. Liu and C.P. Wong, *Adv. Energy Mater.*, 2(2012)884..
26. R.Li, Z.D. Wei and X.L. Gou, *Acs Catal.*, 5(2015) 4133.
27. H.T. Li, Z.H. Kang, Y.Liu and S.T. Lee, *J. Mater Chem.*, 22(2012) 24230.
28. N. Manyala, A. Bello, F. Barzegar, A.A. Khaleed, D.Y. Momodu and J.K. Dangbegnon, *Mater Chem & Phys.*, 182(2016) 139.
29. Q.P. Luo, L. Huang, X. Gao, Y.L. Cheng, B. Yao, Z.M. Hu, J. Wan, X. Xiao and J. Zhou, *Nanotechnology*, 26(2015) 304004.
30. M.S. Wu, M.J. Wang and J.J. Jow, *J. Power Sources*, 195(2010) 3950.